Dancing in the dark: probing Dark Matter through the dynamics of eccentric binary pulsars

Giorgio Nicolini[1,2,3⋆], Andrea Maselli[4,5†] and Miguel Zilhão[2,3,6‡]

1 Montana State University, Bozeman, MT 59717, USA
2 Department of Mathematics, University of Aveiro, 3810-193 Aveiro, Portugal
3 Center for Research and Development in Mathematics and Applications (CIDMA), University of Aveiro, 3810-193 Aveiro, Portugal
4 Gran Sasso Science Institute (GSSI), I-67100 L'Aquila, Italy
5 INFN, Laboratori Nazionali del Gran Sasso, I-67100 Assergi, Italy
6 Department of Physics, University of Aveiro, 3810-193 Aveiro, Portugal

⋆ giorgionicolini@montana.edu , † andrea.maselli@gssi.it , ‡ mzilhao@ua.pt

Abstract

We investigate the dynamics of eccentric binary pulsars embedded in dark matter environments. While previous studies have primarily focused on circular orbits in collisionless dark matter halos, we extend this framework to eccentric systems and explore their interaction with ultralight scalar fields. Adopting a perturbative approach, we compute the modifications to the orbital period induced by dark matter-driven dynamical friction. Our results show that orbital eccentricity amplifies the imprints of non-vacuum environments on binary dynamics, underscoring the potential of such systems as sensitive probes for dark matter signatures.

Contents

1 Introduction

Astrophysical systems do not evolve in isolation. Rather, they interact with complex environments, evolving together with a multitude of matter and fields, possibly of unknown nature. Such environments influence the dynamics of compact objects through mechanisms like accretion, gravitational pull and drag, as well as tidal and gas torques, leaving distinctive imprints across the electromagnetic and gravitational wave (GW) spectra [1, 2]. Such imprints are potentially observable by next-generations GW detectors across a wide range of frequencies [3–7], and by radio telescopes used for pulsar timing arrays [8]. Accurately characterizing these imprints is crucial — not only to avoid systematic biases caused by the incorrect modeling of vacuum templates but also to unlock a deeper understanding of the environments in which black holes and neutron stars evolve. These imprints encode key properties of the surrounding medium, such as its density, viscosity, and spatial scales.

Probing the nature of dark matter (DM) is among the most ambitious scientific goals that can be pursued through the study of these astrophysical settings and their interplay with compact objects. DM remains one of the most enigmatic components of the universe, constituting approximately 27% of its total mass-energy density [9], while continuing to elude direct detection. A major challenge in understanding DM lies in the extraordinary uncertainty surrounding its possible mass scales, which span nearly 80 orders of magnitude. Proposed candidates range from ultralight bosons, such as axions or fuzzy DM with masses as low as 10^{-22} eV [10], to weakly interacting massive particles (WIMPs) at the GeV to TeV scale [11, 12], and even primordial black holes, whose masses span from sub-planetary to supermassive scales [13].

In dense regions near galactic centers, DM tends to cluster around black holes, forming dense "spikes" with density peaks near the black hole horizon [1, 14]. These overdensities modify the dynamics of nearby binaries by altering the gravitational potential and inducing drag forces. Estimates of the local DM density in the Solar neighborhood are typically 0.3 ± 0.1 GeV cm^{-3} [15], but localized density enhancements, such as subhalos or ultracompact clumps, could amplify DM interactions in certain environments.

Previous studies of DM effects on compact binaries can be broadly divided into those involving purely gravitational interactions and those invoking additional non-gravitational couplings. Works focusing on the gravitational influence of ambient DM — through dynamical friction, density spikes, or surrounding halos — which affect the orbital dynamics without requiring any direct coupling to the binary components, include [16–18]. Scenarios based on ultralight scalar fields may also introduce non-gravitational effects, such as resonances or time-dependent scalar interactions, which can produce observable signatures only in the presence of direct couplings [19, 20]. Alternative DM models, including fermionic particles and massive scalar or vector fields, have also been analyzed for their effects on binary pulsar dynamics [21, 22], and the role of spin-2 fields and oscillating ultralight vector fields in these models was investigated in Refs. [23, 24]. Additionally, accreting pulsar-black hole binaries have been suggested as probes for DM properties, with studies providing insights into more exotic DM models [25, 26].

Herein, we will focus exclusively on gravitational drag effects, without assuming any direct coupling between DM and the binary constituents. In fact, observations of double pulsars have been proposed as a novel avenue for investigating the properties of DM in the pulsar's vicinity [16]. DM particles influence the binary dynamics through dynamical friction, which drags the components and induces a secular change in the orbital period. In [16] this effect was investigated for collisionless DM particles, focusing on binaries with circular orbits. There have also been numerous works on the effects of dynamical friction and its interaction with black holes [27–33].

In this work, we continue the investigation of DM detection via binary pulsar timing, extending the analysis of [16] in two key directions. First, we incorporate sources on eccentric orbits, as observed in double pulsar systems [34, 35] and white dwarf–pulsar binaries [36]. Orbital eccen-

tricity is expected to amplify the relative velocity near periastron, thereby enhancing dynamical friction effects [37]. Second, we consider the influence of ultralight DM, which can substantially modify the orbital decay rate compared to the collisionless case. For each scenario, we calculate the induced changes in the orbital period as functions of the binary parameters and evaluate their observability with current and upcoming instruments.

2 Dynamical evolution of binary pulsars

We analyze the interaction between the motion of a binary pulsar and its DM environment using a perturbative approach based on the method of osculating orbits, which is particularly well-suited to study the evolution of binary systems under arbitrary perturbing forces [38], including those induced by DM overdensities. At zeroth order, the binary system in vacuum follows Keplerian dynamics, while environmental effects are treated as first-order perturbations. In this section, we provide a brief overview of the formalism, extending the results of [16] to generic orbits and arbitrary perturbing forces.

2.1 Kepler problem

In the absence of perturbations, the motion of a binary system with total mass $M = m_1 + m_2$ can be described using two reference frames: (a) the *fundamental* (or Galactic) frame, a fixed frame with Cartesian coordinates $\{X, Y, Z\}$; and (b) the *co-rotating* frame, which rotates with a virtual particle of mass $\mu = \frac{m_1 m_2}{M}$ around the system's center of mass. The latter is defined by the coordinates $\{x, y, z\}$, such that the fixed orbital plane coincides with the xy plane, and is accompanied by the constant basis vectors $\boldsymbol{e}_x, \boldsymbol{e}_y, \boldsymbol{e}_z$ and by the time-dependent basis $\boldsymbol{n}, \boldsymbol{\lambda}, \boldsymbol{e}_z$.

The description of the motion relative to the fundamental frame is given in terms of six orbital elements: (i) the semi-latus rectum $p = h^2/(GM)$, where h is the magnitude of the reduced angular momentum, defined as $\boldsymbol{h} = \boldsymbol{r} \times \boldsymbol{v}$; (ii) the eccentricity e, which for bound orbits satisfies $0 \leq e < 1$; (iii) the orbital inclination ι, which specifies the angle between the z-direction of the orbital plane and the Z-direction of the fixed fundamental frame; (iv) the longitude of the ascending node Ω, defined as the angle between the X-axis and the line of nodes, i.e., the intersection of the orbital plane with the fundamental frame; (v) the longitude of pericenter ω, which determines the orientation of the orbit within the orbital plane and is defined as the angle between the pericenter and the line of nodes, measured in the orbital plane; and (vi) the true anomaly $f = \phi - \omega$, that represents the angle between the separation vector and the direction of the pericenter, with ϕ being the azimuthal angle of the body in the orbital plane as measured from the ascending node. In this parametrization, the semi-major axis of the binary orbit is given by $a = \frac{p}{1-e^2}$.

In the co-rotating frame, the displacement vector between the two component masses $\boldsymbol{r} \coloneqq \boldsymbol{r}_2 - \boldsymbol{r}_1$ and its time derivative $\boldsymbol{v}$, read

$$\boldsymbol{r} = r\,\boldsymbol{n}\,, \qquad \boldsymbol{v} = \dot{r}\,\boldsymbol{n} + v_\perp\,\boldsymbol{\lambda}\,, \tag{1}$$

where

$$r = \frac{p}{1 + e\cos f}\,, \qquad \dot{r} = \sqrt{\frac{GM}{p}}\,e\sin f\,, \qquad v_\perp = \sqrt{\frac{GM}{p}}\,(1 + e\cos f)\,, \tag{2}$$

describe the usual Keplerian orbit. The time-dependent basis $\boldsymbol{n}, \boldsymbol{\lambda}, \boldsymbol{e}_z$ can also be expressed in the

fundamental frame as

$$\begin{aligned}\boldsymbol{n} &= [\cos\Omega\cos(\omega+f) - \cos\iota\sin\Omega\sin(\omega+f)]\,\boldsymbol{e}_X + [\sin\Omega\cos(\omega+f) \\ &\quad + \cos\iota\cos\Omega\sin(\omega+f)]\,\boldsymbol{e}_Y + \sin\iota\sin(\omega+f)\,\boldsymbol{e}_Z\,, \qquad (3a)\\ \boldsymbol{\lambda} &= [-\cos\Omega\sin(\omega+f) - \cos\iota\sin\Omega\cos(\omega+f)]\,\boldsymbol{e}_X + [-\sin\Omega\sin(\omega+f) \\ &\quad + \cos\iota\cos\Omega\cos(\omega+f)]\,\boldsymbol{e}_Y + \sin\iota\cos(\omega+f)\,\boldsymbol{e}_Z\,, \qquad (3b)\\ \boldsymbol{e}_z &= \sin\iota\sin\Omega\,\boldsymbol{e}_X - \sin\iota\cos\Omega\,\boldsymbol{e}_Y + \cos\iota\,\boldsymbol{e}_Z\,. \qquad (3c)\end{aligned}$$

2.2 Perturbed Kepler problem

Additional forces perturbing the zeroth-order Keplerian motion cause the orbital elements to evolve over time. These changes can be described with the method of osculating orbits, in which the perturbed trajectory is treated as a sequence of instantaneous Keplerian orbits that match the true motion at every instant. Assuming that the relative acceleration between the two bodies is generically given by

$$\boldsymbol{a} \coloneqq \boldsymbol{a}_2 - \boldsymbol{a}_1 = -\frac{GM}{r^2}\boldsymbol{n} + \boldsymbol{F}\,, \qquad (4)$$

we decompose the perturbing force per unit mass $\boldsymbol{F}$ in the co-rotating frame as

$$\boldsymbol{F} = \mathscr{R}\,\boldsymbol{n} + \mathscr{S}\,\boldsymbol{\lambda} + \mathscr{W}\,\boldsymbol{e}_z\,, \qquad (5)$$

with

$$\mathscr{R} = \boldsymbol{F}\cdot\boldsymbol{n}\,, \quad \mathscr{S} = \boldsymbol{F}\cdot\boldsymbol{\lambda}\,, \quad \mathscr{W} = \boldsymbol{F}\cdot\boldsymbol{e}_z\,. \qquad (6)$$

Following [38], at first order in perturbation theory, the evolution of the orbital elements is then given by

$$\begin{aligned}\frac{dp}{df} &\simeq 2\frac{p^3}{GM}\frac{1}{(1+e\cos f)^3}\mathscr{S}(f), \qquad (7a)\\ \frac{de}{df} &\simeq \frac{p^2}{GM}\left[\frac{\sin f}{(1+e\cos f)^2}\mathscr{R}(f) + \frac{2\cos f + e(1+e\cos^2 f)}{(1+e\cos f)^3}\mathscr{S}(f)\right], \qquad (7b)\\ \frac{d\iota}{df} &\simeq \frac{p^2}{GM}\frac{\cos(\omega+f)}{(1+e\cos f)^3}\mathscr{W}(f), \qquad (7c)\\ \sin\iota\frac{d\Omega}{df} &\simeq \frac{p^2}{GM}\frac{\sin(\omega+f)}{(1+e\cos f)^3}\mathscr{W}(f), \qquad (7d)\\ \frac{d\omega}{df} &\simeq \frac{1}{e}\frac{p^2}{GM}\left[-\frac{\cos f}{(1+e\cos f)^2}\mathscr{R}(f) + \frac{2+e\cos f}{(1+e\cos f)^3}\sin f\,\mathscr{S}(f) - e\cot\iota\frac{\sin(\omega+f)}{(1+e\cos f)^3}\mathscr{W}(f)\right], \qquad (7e)\end{aligned}$$

with

$$\frac{dt}{df} \simeq \sqrt{\frac{p^3}{GM}}\frac{1}{(1+e\cos f)^2}\left[1 - \frac{1}{e}\frac{p^2}{GM}\left(\frac{\cos f}{(1+e\cos f)^2}\mathscr{R}(f) - \frac{2+e\cos f}{(1+e\cos f)^3}\sin f\,\mathscr{S}(f)\right)\right], \qquad (8)$$

where the right-hand side of these equations is understood to be evaluated at the (zeroth-order) Keplerian solution. The coefficients $\mathscr{R}$, $\mathscr{S}$, and $\mathscr{W}$ depend on the specific form of the perturbing force. In the next section we will compute these coefficients for different dynamical friction models.

Equations (7a) and (7b) allow us to obtain the f derivative of the orbital period. With these equations, Kepler's third law $P_b^2 = \frac{4\pi^2}{GM}a^3$ and the relation between p and the semi-major axis a,

$p = a\,(1-e^2)$, we can write

$$\frac{dP_b}{df} \simeq 3P_b \frac{p^2}{GM}\frac{1}{(1-e^2)(1+e\cos f)^2}\left[\frac{1+e\cos f\,(2+e^2\cos f)}{1+e\cos f}\mathscr{S}(f) + e\sin f\,\mathscr{R}(f)\right]. \tag{9}$$

We are interested in *secular changes* of a generic orbital parameter ζ^a and its time derivative, obtained by averaging them over an orbit:

$$\Delta\zeta^a = \int_0^{2\pi}\frac{d\zeta^a}{df}df\,, \quad \langle\dot{\zeta}^a\rangle := \frac{\Delta\zeta^a}{P_b}\,. \tag{10}$$

For the orbital period change (9) this yields

$$\langle\dot{P}_b\rangle = 3\frac{p^2}{GM(1-e^2)}\int_0^{2\pi}\left[\frac{1+e\cos f\,(2+e^2\cos f)}{(1+e\cos f)^3}\mathscr{S}(f) + \frac{e\sin f}{(1+e\cos f)^2}\mathscr{R}(f)\right]df\,. \tag{11}$$

The time derivative of the orbital period, $\dot{P}_b$, is an observable quantity measurable through pulsar timing, encoding information about the astrophysical environment in which pulsars evolve. In the following, we use Eq. (11) as a figure of merit to quantify the impact of DM on their orbital dynamics.

3 The perturbing forces

3.1 Dynamical friction for collisionless dark matter

The dynamical friction force $\boldsymbol{F}_i^{\rm DF}$ experienced by an object of mass m_i in linear motion through a homogeneous collisionless medium of density $\rho_{\rm DM}$ is given by [39,40]

$$\boldsymbol{F}_i^{\rm DF} = -4\pi\rho_{\rm DM}\lambda\frac{G^2m_i^2}{\tilde{v}_i^3}\left[\mathrm{erf}(X_i) - \frac{2X_i}{\sqrt{\pi}}e^{-X_i^2}\right]\tilde{\boldsymbol{v}}_i\,, \tag{12}$$

where $\tilde{\boldsymbol{v}}_i$ denotes the object's velocity relative to the wind of DM particles $\boldsymbol{v}_w$, $X_i := \dfrac{\tilde{v}_i}{\sqrt{2}\sigma}$, with σ being the dispersion of the DM Maxwellian velocity distribution, and $\lambda \approx 20^{+10}_{-10}$ is the Coulomb logarithm[1]. Now, we consider a binary system of masses $m_1 \geq m_2$ and total mass M, affected by dynamical friction in a non-vacuum environment. The displacement vector between the two bodies is $\boldsymbol{r} = \boldsymbol{r}_2 - \boldsymbol{r}_1$, where $\boldsymbol{r}_{1,2}$ are their respective coordinate vectors. Following the approach of [16], we recast Eq. (12)

$$\boldsymbol{F}_i^{\rm DF} = -Ab_i\frac{m_i^2}{M}\tilde{\boldsymbol{v}}_i\,, \quad \text{where} \quad A = 4\pi\rho_{\rm DM}\lambda G^2M\,, \quad b_i = \frac{1}{\tilde{v}_i^3}\left[\mathrm{erf}(X_i) - \frac{2X_i}{\sqrt{\pi}}e^{-X_i^2}\right], \tag{13}$$

and the equations of motion for $\boldsymbol{r}$ and the center-of-mass position $\boldsymbol{R}$ are given by

$$\dot{\boldsymbol{v}} = -\frac{GM}{r^3}\boldsymbol{r} + a_1\eta\,\boldsymbol{v} + a_2(\boldsymbol{v}_w + \boldsymbol{V})\,, \tag{14}$$

$$\dot{\boldsymbol{V}} = a_2\eta\,\boldsymbol{v} + a_3(\boldsymbol{v}_w + \boldsymbol{V})\,, \tag{15}$$

where $\eta = \mu/M = m_1m_2/M^2$ is the symmetric mass ratio, and the coefficients a_1, a_2, and a_3 are defined as

$$a_1 = -A(b_1+b_2)\,, \qquad a_2 = \frac{A}{2}(b_1\Delta_+ + b_2\Delta_-)\,, \qquad a_3 = -\frac{A}{4}\left(b_1\Delta_+^2 + b_2\Delta_-^2\right), \tag{16}$$

[1] We fix $\lambda = 20$ throughout this work for consistency with the existing literature (see e.g. [16]). In any case, since this value appears as an overall factor, all our results can be appropriately rescaled.

where $\Delta_\pm = \Delta \pm 1$, $\Delta = \sqrt{1-4\eta}$. Equations (14)-(15) show that, in the presence of a non-vacuum environment, the binary's center of mass experiences an acceleration due to dynamical friction.

To apply the osculating orbit method, we must separate the zeroth-order (unperturbed) and first-order (perturbed) components of the binary's dynamics. To this aim we introduce the book-keeping parameter $\epsilon := \frac{\rho_{\rm DM}}{M} L^3 \sim \rho_{\rm DM} G P_b^2$, which determines the ratio between friction and the gravitational force, where L is the characteristic orbital separation of the binary, and we use it as perturbative parameter for the method of osculating orbits. For $\epsilon \to 0$ we recover the vacuum binary configuration. We then expand all vectors in Eqs. (14)-(15) as $\boldsymbol{u} = \boldsymbol{u}^{(0)} + \epsilon \boldsymbol{u}^{(1)}$. At zeroth order, $\boldsymbol{V}^{(0)} = 0$; keeping only first-order terms in ϵ, Eq. (14) takes the form

$$\dot{\boldsymbol{v}} = -\frac{GM}{r^2}\boldsymbol{n} + a_1 \eta \boldsymbol{v}^{(0)} + a_2 \boldsymbol{v}_w \,,$$

which does not depend on the movement of the center-of-mass $\boldsymbol{V}$. Comparing this with Eq. (4), we can straightforwardly identify the perturbing force per unit mass, $\boldsymbol{F}$, as

$$\boldsymbol{F} = a_1 \eta \boldsymbol{v}^{(0)} + a_2 \boldsymbol{v}_w \,. \tag{17}$$

To decompose the perturbing force (17) in the form of Eq. (5), we first use the zeroth-order Keplerian solution to orient the Galactic frame such that $\Omega^{(0)} = \omega^{(0)} = \iota^{(0)} = 0$. This choice simplifies the projection of vectors and is made without loss of generality, as physical observables are invariant under coordinate rotation. Then, using Eqs. (3a)-(3c), we obtain the basis vectors $(\boldsymbol{n}, \boldsymbol{\lambda}, \boldsymbol{e}_z)$:

$$\boldsymbol{n}^{(0)} = (\cos f^{(0)},\ \sin f^{(0)},\ 0), \qquad \boldsymbol{\lambda}^{(0)} = (-\sin f^{(0)},\ \cos f^{(0)},\ 0), \qquad \boldsymbol{e}_z^{(0)} = (0,\ 0,\ 1)\,. \tag{18}$$

Given that the velocity vector is expressed as

$$\boldsymbol{v}^{(0)} = \dot{r}^{(0)} \boldsymbol{n}^{(0)} + v_\perp^{(0)} \boldsymbol{\lambda}^{(0)} \,, \tag{19}$$

we obtain

$$\boldsymbol{v}^{(0)} = \left(\dot{r}^{(0)} \cos f^{(0)} + v_\perp^{(0)} \sin f^{(0)}\right) \boldsymbol{e}_X + \left(\dot{r}^{(0)} \sin f^{(0)} + v\perp^{(0)} \cos f^{(0)}\right) \boldsymbol{e}_Y \,. \tag{20}$$

Moreover, we decompose the velocity vector $\boldsymbol{v}_w$ as

$$\boldsymbol{v}_w = v_w\,(\sin\beta\cos\alpha,\ \sin\beta\sin\alpha,\ \cos\beta)\,, \tag{21}$$

which we assume to be constant over the observation period. Here, α and β are the azimuthal and polar angles defining the direction of $\boldsymbol{v}_w$ in the Galactic reference frame. The projection of the perturbing force is then given by

$$\mathscr{R} = \boldsymbol{F}\cdot\boldsymbol{n}^{(0)} = a_1\eta\,\dot{r}^{(0)} + a_2 v_w \sin\beta\cos(f-\alpha)\,, \tag{22a}$$

$$\mathscr{S} = \boldsymbol{F}\cdot\boldsymbol{\lambda}^{(0)} = a_1\eta\, v_\perp^{(0)} - a_2 v_w \sin\beta\sin(f-\alpha)\,, \tag{22b}$$

$$\mathscr{W} = \boldsymbol{F}\cdot\boldsymbol{e}_z^{(0)} = a_2 v_w \cos\beta\,. \tag{22c}$$

Using the (Keplerian) expressions for the radial and orthogonal components of the velocity

$$v_\perp^{(0)} = \sqrt{\frac{GM}{p}}\,(1+e\cos f)\,, \qquad \dot{r}^{(0)} = \sqrt{\frac{GM}{p}}\,e\sin f\,, \tag{23}$$

we finally obtain the explicit form of $\mathscr{S}(f)$ and $\mathscr{R}(f)$, required to compute the shift in the orbital period,

$$\mathscr{S}(f) = a_1\eta\sqrt{\frac{GM}{p}}(1+e\cos f) - a_2 v_w \sin\beta\sin(f-\alpha)\,, \tag{24a}$$

$$\mathscr{R}(f) = a_1\eta\sqrt{\frac{GM}{p}}\,e\sin f + a_2 v_w \sin\beta\cos(f-\alpha)\,. \tag{24b}$$

3.1.1 Validity of the linear motion approximation

Equation (12) was derived for linear motion, but it can also be applied to a binary provided that one can neglect the interaction with the companion's wake. Following [41] and [16], this expression should hold provided that the characteristic size of the wake L is much smaller than the semi-minor axis of the binary orbit b. Estimating L from the size of the gravitational sphere of influence as in [41] and [16], we have the condition $m_{\rm DM}\sigma^2 \sim Gm_i m_{\rm DM}/L$. Using Kepler's law, the condition $L \ll b$ can then be written as

$$P_b \gg \frac{Gm_i}{\sigma^3}\frac{1}{(1-e^2)^{\frac{3}{4}}} \sim \frac{0.46}{(1-e^2)^{\frac{3}{4}}}\left(\frac{m_i}{M_\odot}\right)\left(\frac{150\ \mathrm{km/s}}{\sigma}\right)^3\ \mathrm{day}. \tag{25}$$

We therefore see that, even for very high values of eccentricity of $e \simeq 0.98$, we have

$$P_b \gg 5.2\left(\frac{m_i}{M_\odot}\right)\left(\frac{150\ \mathrm{km/s}}{\sigma}\right)^3\ \mathrm{day},$$

which validates the use of Eq. (12) for orbital periods of $P_b \gtrsim 100$ days. This threshold is satisfied by various known binary pulsars (see, e.g., the ATNF Pulsar Catalogue [42]).

3.2 Dynamical friction for ultra-light dark matter

Considering now an ultralight scalar-field DM model, the friction force was first derived in [43] for non-relativistic velocities, extended in [27] to the relativistic case and also extracted and explored numerically in [28, 29]. This friction arises from the gravitational response of the scalar field medium — a coherent wave — as the object moves through it, generating a trailing density distortion (or wake) that acts back on the object. The expression takes the form

$$\boldsymbol{F}_i^{\rm SF} = -4\pi\rho_{\rm DM}\frac{G^2m_i^2}{\tilde{v}_i^3}\mathscr{C}_i\,\tilde{\boldsymbol{v}}_i \tag{26}$$

where $\mathscr{C}_i$ can be written in a closed formed fashion in different regimes of validity.

Defining the scalar field mass parameter $\mu_{\rm SF} := \frac{m_{\rm SF}c}{\hbar}$ (where $1/\mu_{\rm SF}$ is its reduced Compton wavelength), we introduce the parameter $\alpha_s := \mu_{\rm SF}\frac{GM}{c^2}$, which encodes the effective gravitational coupling between the DM field and the binary. In the limit $\alpha_s \ll 1$, $\alpha_s\frac{c}{\tilde{v}_i} \ll 1$, $\mathscr{C}_i$ takes the form [28, 43]

$$\mathscr{C}_i \simeq \mathrm{Cin}\left(\mu_{\rm SF}\frac{\tilde{v}_i}{c}b_{\max}\right) + \frac{\sin\left(\mu_{\rm SF}\frac{\tilde{v}_i}{c}b_{\max}\right)}{\mu_{\rm SF}\frac{\tilde{v}_i}{c}b_{\max}} - 1 \tag{27}$$

where $\mathrm{Cin}(z) = \int_0^z(1-\cos t)/t\ dt$ is the cosine integral and $b_{\max} = 2R$, given by twice the cutoff radius, represents an infrared cutoff which regularizes the long-range nature of the interaction and depends on the effective size of the perturbed DM region. In the following, we set the cutoff radius R to the semi-minor axis of the binary orbit, which represents the characteristic spatial scale over which each component of the binary perturbs the surrounding DM environment [28, 29, 43]. Similarly to previous sections, we can rewrite Eq. (26) as

$$\boldsymbol{F}_i^{\rm SF} = -A^{\rm SF}\frac{m_i^2}{M}b_i^{\rm SF}\tilde{\boldsymbol{v}}_i, \quad A^{\rm SF} = 4\pi\rho_{\rm DM}G^2M, \quad b_i^{\rm SF} = \frac{\mathscr{C}_i}{\tilde{v}_i^3}\,. \tag{28}$$

We can follow once again the same steps as before to obtain the projections of the perturbing force $\mathscr{S}(f)$ and $\mathscr{R}(f)$ due to scalar-field DM by taking Eqs. (24) and replacing the coefficients $a_{1,2}$ with their corresponding values from Eq. (28).

4 Changes in the orbital period due to Dark Matter

We now apply the expressions derived in the previous section to estimate the change in the orbital period of a binary system under various DM models. We remark that, while the dynamical friction formulas were originally developed for linear motion, as discussed in Sec. 3.1.1, they provide reasonable approximations for systems with sufficiently large orbital periods. We therefore adopt them here as proxies to model systems in bound orbital configurations satisfying condition (25).[2]

The DM density appears as an overall scaling factor in the expressions for the perturbing forces (13) and (28), and consequently in the expression for the period derivative (11). For convenience, we will perform all our computations using a reference value of $\rho_0 = 1\ \mathrm{GeV\,cm^{-3}}$, which is the order of magnitude estimated for the local DM density from recent observations [44]. For the velocity v_w and velocity dispersion σ of the DM wind we will explore different values around the typically used order of magnitude of v_w, $\sigma \sim 100$ km/s [45–47].

We begin our analysis by examining the collisionless DM scenario described in Sec. 3.1. Figure 1 illustrates the variation in the orbital period as a function of the angle α for binary systems with $P_b = 100$ days on eccentric orbits. Here we fix $\beta = \pi/2$, corresponding to a DM wind flowing parallel to the orbital plane. We explore different values for both the DM wind velocity v_w and the velocity dispersion σ. To facilitate comparison with previous studies, we adopt the same component masses used in [16], namely $m_1 = 1.3M_\odot$ and $m_2 = 0.3M_\odot$.[3]

In contrast to circular orbits, whose secular variations do not depend on α [16], eccentric binaries exhibit a more structured dependence of $\dot{P}_b$. For $\sigma = 50\,\mathrm{km/s}$ (left panel of Fig. 1), systems with relatively large eccentricity, $e \gtrsim 0.5$, display an orbital-period derivative that increases monotonically as α varies over the interval $[0, \pi/2]$. Increasing the velocity dispersion (right panel) introduces additional structure: in this case, $|\dot{P}_b|$ tends to decrease initially and then rise again as α increases, with the location of the turning point depending on e. For smaller eccentricities, this behavior is absent irrespective of σ, and $\dot{P}_b$ remains approximately constant or shows a mild decrease as α varies. Larger values of σ also lead to an overall suppression of $\dot{P}_b$. By comparison, increasing v_w produces only a modest reduction in $|\dot{P}_b|$, without modifying the qualitative trends discussed above.

Overall, in contrast to the circular case, the dependence of $\dot{P}_b$ on the system parameters for elliptical orbits underscores the importance of accounting for orbital eccentricity when assessing the impact of dark matter on the dynamics of binary pulsars.

Figure 2 further compares the secular evolution of P_b for circular and eccentric binaries across different orbital and DM parameters as computed from Eq. (11). In Fig. 2, solid and dashed curves, enclosed within shaded bands, correspond to orbital periods of $P_b = 100$ days and $P_b = 200$ days, respectively. For a fixed value of α, the orbital-period derivative in eccentric systems can differ from the circular-orbit case by up to two orders of magnitude. At the lowest velocity dispersion considered, $\sigma = 50$ km/s, $\dot{P}_b$ may exceed its circular counterpart by roughly one order of magnitude for $e = 0.7$, and by two orders or magnitude for $e = 0.9$. For the smallest eccentricity examined, $e = 0.3$, the ratio $|\dot{P}_b/\dot{P}_b^{e=0}|$ falls below unity, decreasing monotonically with α when $P_b = 200$, and developing a turning point when $P_b = 100$.

Consistent with Fig. 1, variations in v_w have only a limited impact, although $|\dot{P}_b/\dot{P}_b^{e=0}|$ remains $\gtrsim 1$ for all eccentricities when v_w is sufficiently low. Allowing for $\sigma > 50$ km/s at fixed v_w introduces additional structure: the ratio now develops a turning point and can change sign as α varies, even for $e = 0.7$ and $e = 0.9$. This behavior gradually disappears as v_w increases, with variations in the orbital period of eccentric systems consistently exceeding those of circular ones.

[2] The bound derived in Sec. 3.1.1 is strictly valid for the collisionless DM model. For simplicity, however, we will apply this criterion to the other environmental models we consider.

[3] The results for zero eccentricity match those shown in Fig. 3 of Ref. [16] when rescaled using the DM density $\rho_{\rm DM} = 2 \times 10^3\ \mathrm{GeV\,cm^{-3}}$ employed therein.

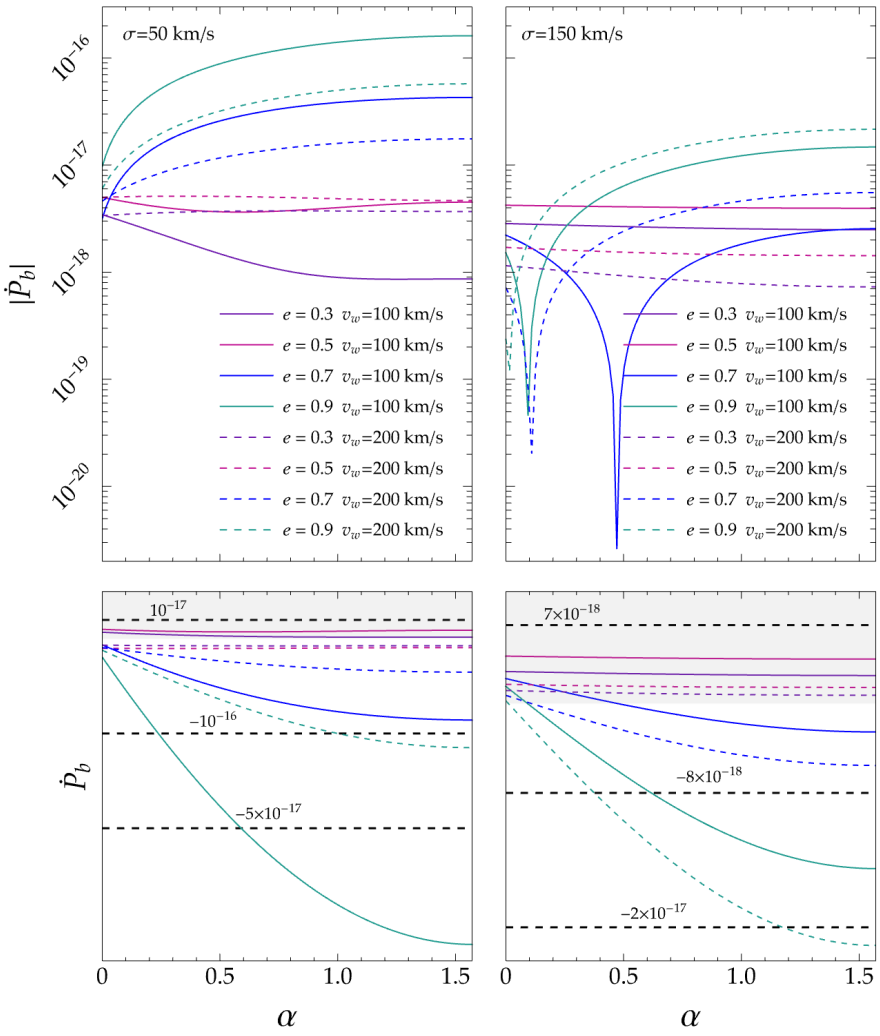

Figure 1: (Top Row) Absolute value of the secular change in the orbital period as a function of α for binary pulsars with $m_1 = 1.3M_\odot$ and $m_2 = 0.3M_\odot$ and different values of eccentricity. For all configurations we assume $\beta = \pi/2$ and $P_b = 100$ days. Solid and dashed curves refer to DM wind speed of $v_w = 100$ km/s and $v_w = 200$ km/s, while left and right panel to velocity dispersion of $\sigma = 50$ km/s and $\sigma = 150$ km/s, respectively. (Bottom Row) Secular change in the orbital period for the same configurations shown in the top panels. Horizontal dashed black lines identify specific values of $\dot{P}_b$. Gray and white regions correspond to parameter space in which $\dot{P}_b > 0$ and $\dot{P}_b < 0$, respectively.

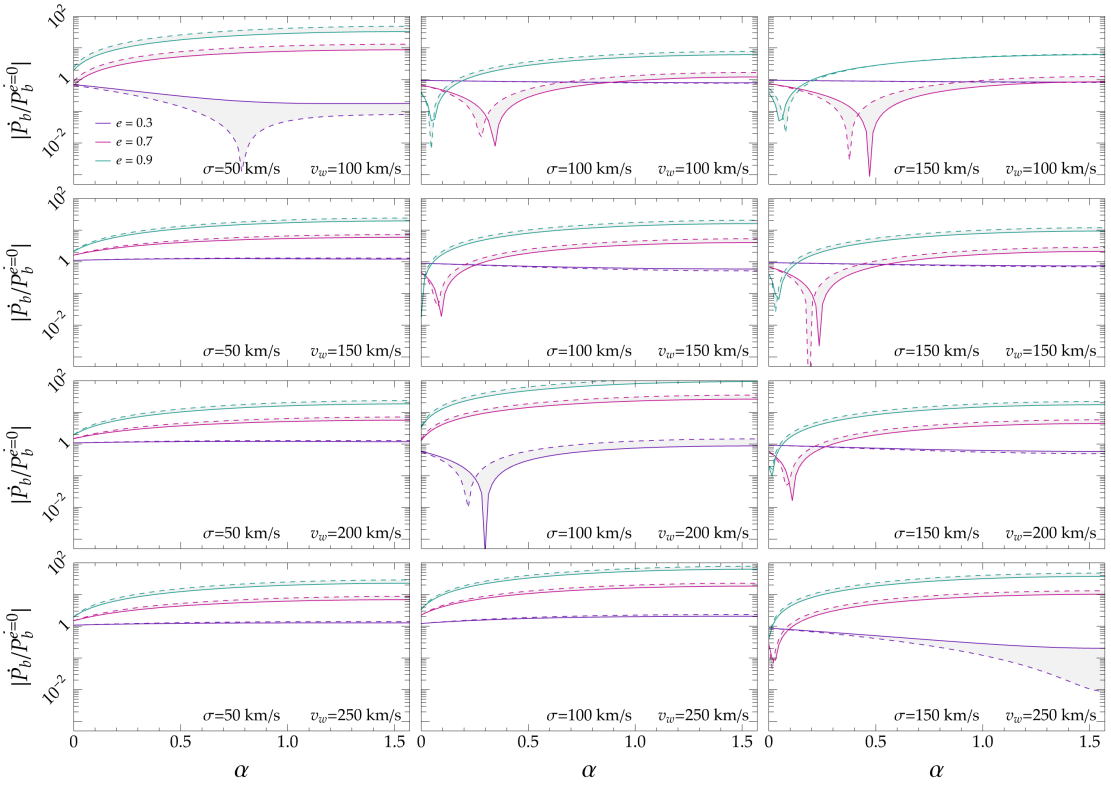

Figure 2: Secular change in the orbital period as given from Eq. (11) for binaries on eccentric orbits, normalized to the circular case, as a function of the angle α. Each panel corresponds to a different choice of the DM wind velocity v_w and of the velocity dispersion σ. Values of $\dot{P}_b$ are obtained for a binary pulsar with component masses $m_1 = 1.3M_\odot$ and $m_2 = 0.3M_\odot$. The lower solid (upper dashed) curve of each colored band identify binaries with orbital period of $P_b = 100$ ($P_b = 200$) days. For all panels we fix $\beta = \pi/2$.

Configurations with $e = 0.3$ generally yield $|\dot{P}_b/\dot{P}_b^{e=0}| \sim 1$, although for the largest values of σ and v_w considered, the trend reverses and changes in P_b become larger in the circular case.

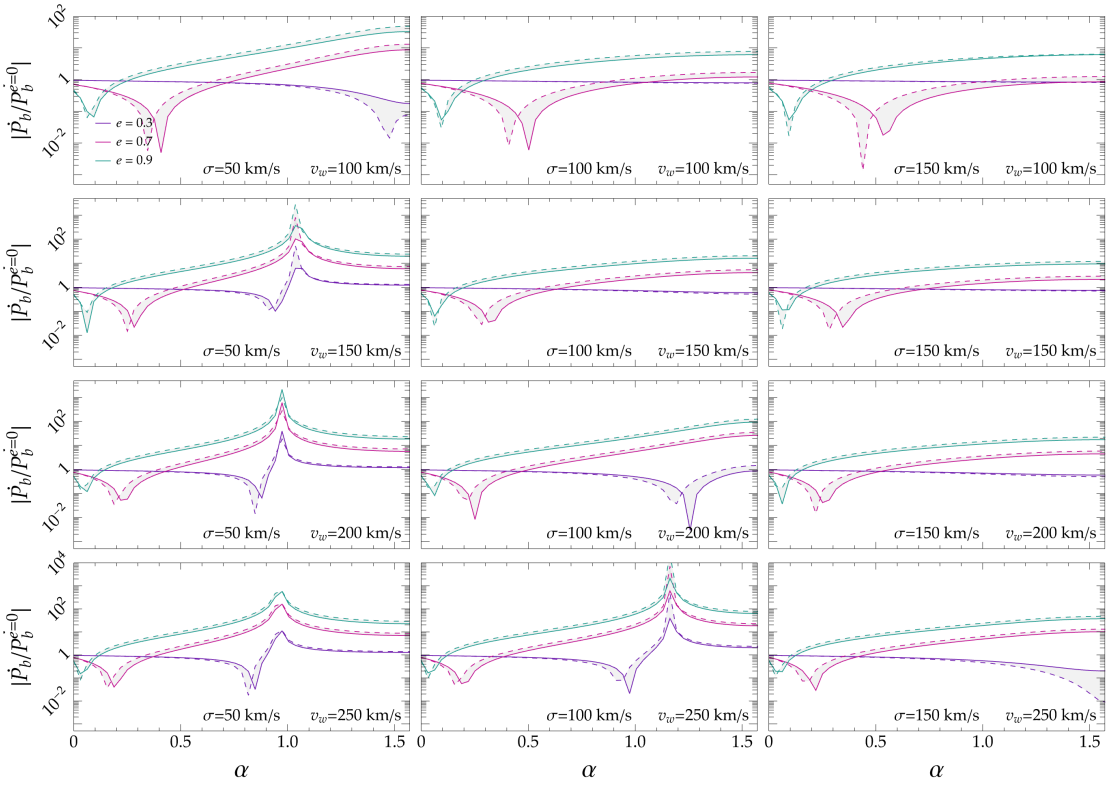

Figure 3: Same as Fig. 2 but fixing $\alpha = \pi/2$ and varying β.

Figure 3 shows the values of $\dot{P}_b$ as a function of β, fixing $\alpha = \pi/2$, for the same component masses and orbital configurations considered in Fig. 1. The overall behavior of $\dot{P}_b$ is consistent with the trends discussed above: the eccentricity produces a clear splitting in the secular change for a given β, leading to substantial deviations from the circular case examined in [16]. Variations in β, however, generate a more intricate structure than those in α, with the ratio $|\dot{P}_b/\dot{P}_b^{e=0}|$ developing multiple turning points as β varies.

To assess the dependence of $\dot{P}_b$ on the component masses, we varied $m_{1,2}$ and found that their influence on the results is generally smaller than an order of magnitude. Figure 4 displays density plots of the ratio $|\dot{P}_b/\dot{P}_b^{e=0}|$ as a function of m_1 and the mass ratio $q = m_2/m_1$, assuming $\alpha = \beta = \pi/2$, $P_b = 100$ days, and $(\sigma, v_w) = (100, 250)$ km/s. The left and right panels correspond to binaries with $e = 0.3$ and $e = 0.9$, respectively.

For $e = 0.3$, the ratio $|\dot{P}_b/\dot{P}_b^{e=0}|$ drops well below unity as the system becomes increasingly asymmetric, i.e. for $q \ll 1$. In contrast, for $e = 0.9$, the orbital period changes exceed those of the circular case across the full parameter range, with the smallest differences occurring near equal masses, $q \sim 1$.

We now turn to the ultra-light dark matter scenario described in Sec. 3.2, adopting the friction coefficient $\mathscr{C}_i$ given in Eq. (27), which applies in the low-velocity and small-α_s regime [43]. In this case, the prospects for observing changes in the orbital period are less favorable than in the collisionless DM scenario. For the component masses considered above, $m_1 = 1.3\,M_\odot$ and $m_2 = 0.3\,M_\odot$, and an orbital period of $P_b = 100$ days, we find typical values $|\dot{P}_b| \lesssim 10^{-20}$ for $\mu_{\rm SF} \lesssim 10^{-8}\,{\rm m}^{-1}$, with the magnitude of the orbital period change increasing mildly with the scalar-field mass.

Larger boson masses are limited by the range of validity of the small-coupling approximation

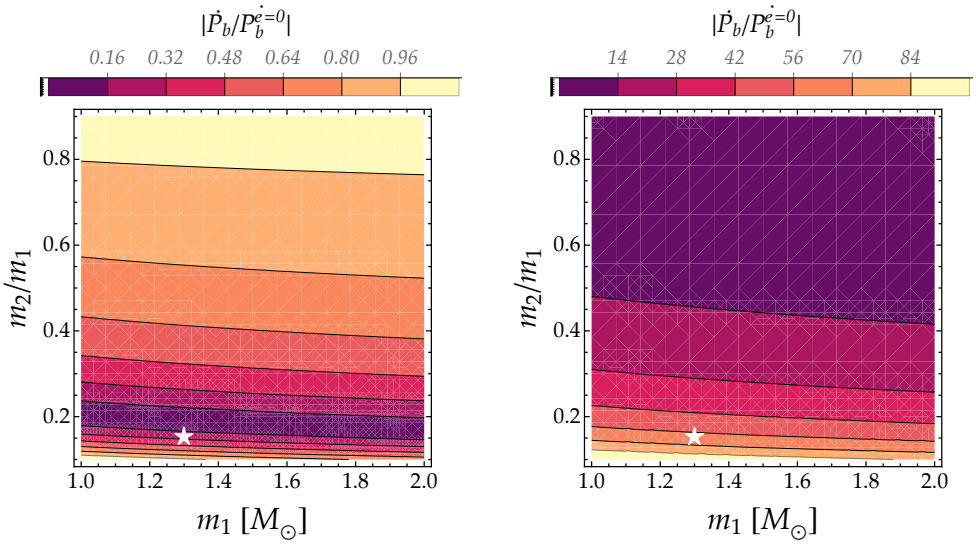

Figure 4: Density plots for the change in the orbital period for binaries on eccentric orbits (left panel: $e = 0.3$; right panel: $e = 0.9$), normalized to the circular case, as a function of m_1 and the mass ratio m_2/m_1. In both panels, we fix $\alpha = \beta = \pi/2$, $P_b = 100$ days, $\sigma = 100$ km/s, and $v_w = 250$ km/s. The yellow star identifies the case discussed in Figs. 1–2, with $m_1 = 1.3\,M_\odot$ and $m_2 = 0.3\,M_\odot$.

underlying Eq. (27). The resulting values of $\dot{P}_b$ are nearly insensitive to the angles (α, β), the velocity v_w, and, notably, the binary eccentricity. Although somewhat larger effects can be obtained for systems with longer orbital periods, even for $P_b = 500$ days we find $|\dot{P}_b| \lesssim 10^{-18}$, still with no appreciable dependence on the eccentricity.

5 Final remarks

In this study, we investigated the dynamics of eccentric binary pulsars evolving in DM-rich environments. We computed changes in the orbital period due to dynamical friction induced by the surrounding medium, modeled either as collisionless or ultralight DM. For each DM scenario, we explored the binary parameter space, analyzing how variations in the orbital period depend on both the properties of the environment and the orbital configuration. Our results show that the impact of DM on the orbital evolution of binary pulsars depends sensitively on the underlying microphysical model. While collisionless DM can induce sizable, eccentricity-dependent modifications of the orbital period, the ultralight scalar-field scenario leads to significantly weaker effects, with a reduced sensitivity to orbital parameters and system properties.

In the collisionless scenario, orbital eccentricity significantly amplifies the effects of dynamical friction, enhancing them by more than an order of magnitude compared to circular orbits. Depending on the relative orientation of the binary with respect to the DM wind, $\dot{P}_b$ can change sign, with turning points dictated by the eccentricity and by the properties of the DM distribution, such as the velocity dispersion.

From an observational perspective, it is crucial to account for the intrinsic derivative of the orbital period, which includes contributions from kinematic effects due to the relative acceleration between the binary pulsar and the Solar System barycenter, as well as the energy loss due to gravitational-wave emission. The kinematic contributions alone can reach values of order $\dot{P}_b^{\rm intr} \sim 10^{-15}$, requiring precise knowledge of the pulsar distance for reliable subtraction [48]. To

isolate the effect of dynamical friction, it is therefore advantageous to consider systems in which the orbital decay driven by GW emission is subdominant. This typically occurs in binaries with longer orbital periods; however, such systems also pose observational challenges, as measuring $\dot{P}_b$ with high precision becomes increasingly difficult at large orbital periods.

Current pulsar-timing experiments already achieve remarkable precision in measuring $\dot{P}_b$ for compact and highly relativistic binaries. Indeed, measurements in systems such as PSR B1913+16 and the double pulsar J0737−3039A/B report fractional uncertainties as low as $\sigma_{\dot{P}_b}/|\dot{P}_b| \sim 10^{-4}$–$10^{-5}$ [49, 50]. This level of precision is not yet attainable for the wider binaries considered here, with $P_b \gtrsim 100$ days, for which intrinsic orbital-period derivatives are often not reported in the ATNF Pulsar Catalogue [42]. Nevertheless, this situation is expected to improve substantially with next-generation facilities such as the Square Kilometre Array (SKA), whose enhanced sensitivity, expanded pulsar census, and extended timing baselines are expected to enable significantly more precise determinations of $\dot{P}_b$ in long-period binaries than currently achievable ones [51, 52].

Using the binary pulsar PSR J1302−6350 [42,53] as a representative example, with parameters $m_1 \simeq 20\,M_\odot$, $m_2 \simeq 1.4\,M_\odot$, eccentricity $e \simeq 0.87$, and orbital period $P_b \simeq 1237$ days, our collisionless DM model predicts a variation in the orbital period due to dynamical friction of $\dot{P}_b \simeq 6.7 \times 10^{-15}$ for $v_w = 250$ km/s, and $\dot{P}_b \simeq 1.8 \times 10^{-14}$ for $v_w = 150$ km/s, assuming reference values $\sigma = 50$ km/s, $\alpha = \beta = \pi/2$, and $\rho_0 = 1$ GeV cm^{-3} for the DM density.[4] These values have the opposite sign and are more than an order of magnitude larger than the orbital decay expected from gravitational-wave emission in this system, $\dot{P}_b^{\rm GW} \simeq -7.7 \times 10^{-16}$, indicating that dynamical friction could dominate the secular evolution of the orbit in such wide and highly eccentric binaries.

For typical Solar-neighborhood DM densities of $\rho_\odot \sim 0.3$ GeV cm^{-3} [44], the resulting effect on the orbital period would be challenging to detect. However, in regions with higher DM densities, such as the Galactic Center—where estimates suggest $\rho_{\rm DM} \sim 10^2$ GeV cm^{-3} at distances of 100 pc from the center and up to $\rho_{\rm DM} \sim 10^3$ GeV cm^{-3} at 10 pc [54, 55]—these effects are expected to be amplified and could potentially be measurable [17]. Additionally, as noted in [56], binaries located in regions of enhanced DM density may also provide improved sensitivity to accretion-based effects. Recently reported systems such as the millisecond binary pulsar PSR J1744−2946 [57], located within 140 pc of the Galactic Center, exemplify promising targets for future observational constraints.

Looking ahead, next-generation facilities such as the SKA are expected to detect thousands of new pulsars, with the goal of uncovering the majority of the Galactic population [51, 52]. As more binary pulsars are discovered, particularly those with high eccentricities and/or located in DM-rich environments, the prospects for detecting or constraining dynamical-friction effects will improve substantially. Our results provide a framework for interpreting such future measurements and highlight classes of systems in which these signals may be within reach of next-generation timing arrays.

Acknowledgements

We thank the anonymous referee for their valuable comments which have improved the quality of our manuscript. We also thank Rodrigo Vicente for helpful discussions and Paolo Pani for having carefully read the manuscript and for useful comments. M.Z. further thanks Paulo Teixeira and José Manuel Mota for discussions.

Funding information G.N. and M.Z. acknowledge financial support by the Center for Research and Development in Mathematics and Applications (CIDMA) through Fundação para a

[4] From Eq. (13), $\dot{P}_b$ scales linearly with the DM density.

Ciência e a Tecnologia (FCT) Multi-Annual Financing Program for R&D Units through grants UID/4106/2025 (https://doi.org/10.54499/UID/04106/2025) and UID/PRR/4106/2025 as well as the following projects: PTDC/FIS-AST/3041/2020 (http://doi.org/10.54499/PTDC/FIS-AST/3041/2020); 2022.04560.PTDC (https://doi.org/10.54499/2022.04560.PTDC); and 2022.00721.CEECIND (https://doi.org/10.54499/2022.00721.CEECIND/CP1720/CT0001). A.M. acknowledges financial support from MUR PRIN Grant No. 2022-Z9X4XS, funded by the European Union — Next Generation EU.

References

[1] P. Gondolo and J. Silk, *Dark matter annihilation at the galactic center*, Phys. Rev. Lett. **83**, 1719 (1999), doi:10.1103/PhysRevLett.83.1719, astro-ph/9906391.

[2] E. Barausse, V. Cardoso and P. Pani, *Can environmental effects spoil precision gravitational-wave astrophysics?*, Physical Review D **89**(10), 104059 (2014), doi:10.1103/PhysRevD.89.104059.

[3] A. Abac *et al.*, *The Science of the Einstein Telescope* (2025), 2503.12263.

[4] A. Corsi *et al.*, *Multi-messenger astrophysics of black holes and neutron stars as probed by ground-based gravitational wave detectors: from present to future*, Front. Astron. Space Sci. **11**, 1386748 (2024), doi:10.3389/fspas.2024.1386748, 2402.13445.

[5] M. Colpi *et al.*, *LISA Definition Study Report* (2024), 2402.07571.

[6] J. Luo *et al.*, *Fundamental Physics and Cosmology with TianQin* (2025), 2502.20138.

[7] P. Ajith *et al.*, *The Lunar Gravitational-wave Antenna: mission studies and science case*, JCAP **01**, 108 (2025), doi:10.1088/1475-7516/2025/01/108, 2404.09181.

[8] M. Kramer, D. C. Backer, J. M. Cordes, T. J. W. Lazio, B. W. Stappers and S. Johnston, *Strong-field tests of gravity using pulsars and black holes*, New Astron. Rev. **48**, 993 (2004), doi:10.1016/j.newar.2004.09.020, astro-ph/0409379.

[9] N. Aghanim *et al.*, *Planck 2018 results. VI. Cosmological parameters*, Astron. Astrophys. **641**, A6 (2020), doi:10.1051/0004-6361/201833910, [Erratum: Astron.Astrophys. 652, C4 (2021)], 1807.06209.

[10] D. J. E. Marsh, *Axion Cosmology*, Phys. Rept. **643**, 1 (2016), doi:10.1016/j.physrep.2016.06.005, 1510.07633.

[11] G. Bertone and T. M. P. Tait, *A new era in the search for dark matter*, Nature **562**, 51 (2018), doi:10.1038/s41586-018-0542-z.

[12] L. Roszkowski, E. M. Sessolo and S. Trojanowski, *WIMP dark matter candidates and searches—current status and future prospects*, Rept. Prog. Phys. **81**(6), 066201 (2018), doi:10.1088/1361-6633/aab913, 1707.06277.

[13] B. Carr, F. Kühnel and L. Visinelli, *Constraints on primordial black holes from the galactic gamma-ray background*, Physical Review D **103**(4), 043017 (2021), doi:10.1103/PhysRevD.103.043017.

[14] L. Sadeghian, F. Ferrer and C. M. Will, *Dark matter distributions around massive black holes: A general relativistic analysis*, Phys. Rev. D **88**(6), 063522 (2013), doi:10.1103/PhysRevD.88.063522, 1305.2619.

[15] J. I. Read, *The Local Dark Matter Density*, J. Phys. G **41**, 063101 (2014), doi:10.1088/0954-3899/41/6/063101, 1404.1938.

[16] P. Pani, *Binary pulsars as dark-matter probes*, Phys. Rev. D **92**(12), 123530 (2015), doi:10.1103/PhysRevD.92.123530, 1512.01236.

[17] A. Caputo, J. Zavala and D. Blas, *Binary pulsars as probes of a Galactic dark matter disk*, Phys. Dark Univ. **19**, 1 (2018), doi:10.1016/j.dark.2017.10.005, 1709.03991.

[18] A. Chowdhuri, R. K. Singh, K. Kangsabanik and A. Bhattacharyya, *Gravitational radiation from hyperbolic encounters in the presence of dark matter*, Phys. Rev. D **109**(12), 124056 (2024), doi:10.1103/PhysRevD.109.124056, 2306.11787.

[19] D. Blas, D. López Nacir and S. Sibiryakov, *Secular effects of ultralight dark matter on binary pulsars*, Phys. Rev. D **101**(6), 063016 (2020), doi:10.1103/PhysRevD.101.063016, 1910.08544.

[20] P. Kůs, D. López Nacir and F. R. Urban, *Bayesian sensitivity of binary pulsars to ultra-light dark matter*, Astron. Astrophys. **690**, A51 (2024), doi:10.1051/0004-6361/202449953, 2402.04099.

[21] L. G. Gómez, *Constraining light fermionic dark matter with binary pulsars*, Phys. Dark Univ. **26**, 100343 (2019), doi:10.1016/j.dark.2019.100343, 1906.10316.

[22] B. C. Seymour and K. Yagi, *Probing massive scalar and vector fields with binary pulsars*, Phys. Rev. D **102**(10), 104003 (2020), doi:10.1103/PhysRevD.102.104003, 2007.14881.

[23] J. M. Armaleo, D. López Nacir and F. R. Urban, *Binary pulsars as probes for spin-2 ultra-light dark matter*, JCAP **01**, 053 (2020), doi:10.1088/1475-7516/2020/01/053, 1909.13814.

[24] D. López Nacir and F. R. Urban, *Vector Fuzzy Dark Matter, Fifth Forces, and Binary Pulsars*, JCAP **10**, 044 (2018), doi:10.1088/1475-7516/2018/10/044, 1807.10491.

[25] A. Akil and Q. Ding, *A dark matter probe in accreting pulsar-black hole binaries*, JCAP **09**, 011 (2023), doi:10.1088/1475-7516/2023/09/011, 2304.08824.

[26] I. Goldman, *Astrophysical bounds on mirror dark matter derived from binary pulsars timing data*, In *Cosmology on Small Scales 2020: Excessive Extrapolations and Selected Controversies in Cosmology* (2020), 2011.12070.

[27] R. Vicente and V. Cardoso, *Dynamical friction of black holes in ultralight dark matter*, Phys. Rev. D **105**(8), 083008 (2022), doi:10.1103/PhysRevD.105.083008, 2201.08854.

[28] D. Traykova, K. Clough, T. Helfer, E. Berti, P. G. Ferreira and L. Hui, *Dynamical friction from scalar dark matter in the relativistic regime*, Phys. Rev. D **104**(10), 103014 (2021), doi:10.1103/PhysRevD.104.103014, 2106.08280.

[29] D. Traykova, R. Vicente, K. Clough, T. Helfer, E. Berti, P. G. Ferreira and L. Hui, *Relativistic drag forces on black holes from scalar dark matter clouds of all sizes*, Phys. Rev. D **108**(12), L121502 (2023), doi:10.1103/PhysRevD.108.L121502, 2305.10492.

[30] B. Kocsis, N. Yunes and A. Loeb, *Observable Signatures of EMRI Black Hole Binaries Embedded in Thin Accretion Disks*, Phys. Rev. D **84**, 024032 (2011), doi:10.1103/PhysRevD.86.049907, 1104.2322.

[31] N. Speeney, E. Berti, V. Cardoso and A. Maselli, *Black holes surrounded by generic matter distributions: Polar perturbations and energy flux*, Phys. Rev. D **109**(8), 084068 (2024), doi:10.1103/PhysRevD.109.084068, 2401.00932.

[32] V. Cardoso, T. Ikeda, R. Vicente and M. Zilhão, *Parasitic black holes: The swallowing of a fuzzy dark matter soliton*, Phys. Rev. D **106**(12), L121302 (2022), doi:10.1103/PhysRevD.106.L121302, 2207.09469.

[33] Z. Zhong, V. Cardoso, T. Ikeda and M. Zilhão, *Piercing of a solitonic boson star by a black hole*, Phys. Rev. D **108**(8), 084051 (2023), doi:10.1103/PhysRevD.108.084051, 2307.02548.

[34] E. Fonseca, I. H. Stairs and S. E. Thorsett, *A Comprehensive Study of Relativistic Gravity using PSR B1534+12*, Astrophys. J. **787**, 82 (2014), doi:10.1088/0004-637X/787/1/82, 1402.4836.

[35] D. Mata Sánchez, A. G. Istrate, M. H. van Kerkwijk, R. P. Breton and D. L. Kaplan, *PSR J1012+5307: a millisecond pulsar with an extremely low-mass white dwarf companion*, Mon. Not. Roy. Astron. Soc. **494**(3), 4031 (2020), doi:10.1093/mnras/staa983, 2004.02901.

[36] J. Antoniadis, C. G. Bassa, N. Wex, M. Kramer and R. Napiwotzki, *A white dwarf companion to the relativistic pulsar PSR J1141-6545*, Mon. Not. Roy. Astron. Soc. **412**, 580 (2011), doi:10.1111/j.1365-2966.2010.17929.x, 1011.0926.

[37] B. Bar-Or, G. Kupi and T. Alexander, *Stellar Energy Relaxation around A Massive Black Hole*, Astrophys. J. **764**, 52 (2013), doi:10.1088/0004-637X/764/1/52, 1209.4594.

[38] E. Poisson and C. Will, *Gravity: Newtonian, Post-Newtonian, Relativistic*, Cambridge University Press, ISBN 9781107032866 (2014).

[39] S. Chandrasekhar, *Dynamical Friction. I. General Considerations: the Coefficient of Dynamical Friction*, Astrophys. J. **97**, 255 (1943), doi:10.1086/144517.

[40] S. Chandrasekhar, *Brownian motion, dynamical friction, and stellar dynamics*, Rev. Mod. Phys. **21**, 383 (1949), doi:10.1103/RevModPhys.21.383.

[41] J. D. Bekenstein and R. Zamir, *Dynamical Friction in Binary Systems*, Astrophys. J. Lett. **359**, 427 (1990), doi:10.1086/169075.

[42] R. N. Manchester, G. B. Hobbs, A. Teoh and M. Hobbs, *The Australia Telescope National Facility pulsar catalogue*, Astron. J. **129**, 1993 (2005), doi:10.1086/428488, https://www.atnf.csiro.au/research/pulsar/psrcat/, astro-ph/0412641.

[43] L. Hui, J. P. Ostriker, S. Tremaine and E. Witten, *Ultralight scalars as cosmological dark matter*, Phys. Rev. D **95**(4), 043541 (2017), doi:10.1103/PhysRevD.95.043541, 1610.08297.

[44] P. F. de Salas and A. Widmark, *Dark matter local density determination: recent observations and future prospects*, Rept. Prog. Phys. **84**(10), 104901 (2021), doi:10.1088/1361-6633/ac24e7, 2012.11477.

[45] D. G. Cerdeno and A. M. Green, *Direct detection of WIMPs* pp. 347–369 (2010), doi:10.1017/CBO9780511770739.018, 1002.1912.

[46] L. Lancaster, C. Giovanetti, P. Mocz, Y. Kahn, M. Lisanti and D. N. Spergel, *Dynamical Friction in a Fuzzy Dark Matter Universe*, JCAP **01**, 001 (2020), doi:10.1088/1475-7516/2020/01/001, 1909.06381.

[47] G. Battaglia, A. Helmi, H. Morrison, P. Harding, E. W. Olszewski, M. Mateo, K. C. Freeman, J. Norris and S. A. Shectman, *The Radial velocity dispersion profile of the Galactic Halo: Constraining the density profile of the dark halo of the Milky Way*, Mon. Not. Roy. Astron. Soc. **364**, 433 (2005), doi:10.1111/j.1365-2966.2005.09367.x, [Erratum: Mon.Not.Roy.Astron.Soc. 370, 1055 (2006)], astro-ph/0506102.

[48] H. Hu, *Unlocking Gravity and Gravitational Waves with Radio Pulsars: Advances and Challenges* (2025), 2507.10221.

[49] J. M. Weisberg and Y. Huang, *Relativistic Measurements from Timing the Binary Pulsar PSR B1913+16*, Astrophys. J. **829**(1), 55 (2016), doi:10.3847/0004-637X/829/1/55, 1606.02744.

[50] M. Kramer *et al.*, *Tests of general relativity from timing the double pulsar*, Science **314**, 97 (2006), doi:10.1126/science.1132305, astro-ph/0609417.

[51] M. Kramer and I. H. Stairs, *Strong-field tests of gravity using pulsars and black holes*, Living Reviews in Relativity **18**(1), 1 (2015).

[52] E. F. Keane and et al., *A cosmic census of radio pulsars with the ska*, In *Proceedings of Science, Advancing Astrophysics with the Square Kilometre Array (AASKA14)*, vol. 040 (2015).

[53] R. M. Shannon, S. Johnston and R. N. Manchester, *The kinematics and orbital dynamics of the PSR B1259−63/LS 2883 system from 23 yr of pulsar timing*, Mon. Not. Roy. Astron. Soc. **437**(4), 3255 (2014), doi:10.1093/mnras/stt2123, 1311.0588.

[54] Z.-Q. Shen, G.-W. Yuan, C.-Z. Jiang, Y.-L. S. Tsai, Q. Yuan and Y.-Z. Fan, *Exploring dark matter spike distribution around the Galactic centre with stellar orbits*, Mon. Not. Roy. Astron. Soc. **527**(2), 3196 (2023), doi:10.1093/mnras/stad3282, 2303.09284.

[55] Y. Sofue, *Rotation Curve of the Milky Way and the Dark Matter Density*, Galaxies **8**(2), 37 (2020), doi:10.3390/galaxies8020037, 2004.11688.

[56] A. K. Mishra, *Can Orbital Decay of Accreting Binary Pulsars Probe Dark Matter?* (2025), 2507.06178.

[57] M. E. Lower, S. Dai, S. Johnston and E. D. Barr, *A Millisecond Pulsar Binary Embedded in a Galactic Center Radio Filament*, Astrophys. J. Lett. **967**(1), L16 (2024), doi:10.3847/2041-8213/ad4866, 2404.09098.